Federated Learning With Cooperating Devices: A Consensus Approach for Massive IoT Networks

Stefano Savazzi, *Member, IEEE*, Monica Nicoli, *Member, IEEE*, and Vittorio Rampa, *Member, IEEE*

***Abstract*—Federated learning (FL) is emerging as a new paradigm to train machine learning (ML) models in distributed systems. Rather than sharing and disclosing the training data set with the server, the model parameters (e.g., neural networks' weights and biases) are optimized collectively by large populations of interconnected devices, acting as local learners. FL can be applied to power-constrained Internet of Things (IoT) devices with slow and sporadic connections. In addition, it does not need data to be exported to third parties, preserving privacy. Despite these benefits, a main limit of existing approaches is the centralized optimization which relies on a server for aggregation and fusion of local parameters; this has the drawback of a single point of failure and scaling issues for increasing network size. This article proposes a fully distributed (or serverless) learning approach: the proposed FL algorithms leverage the cooperation of devices that perform data operations inside the network by iterating local computations and mutual interactions via consensus-based methods. The approach lays the groundwork for integration of FL within 5G and beyond networks characterized by decentralized connectivity and computing, with intelligence distributed over the end devices. The proposed methodology is verified by the experimental data sets collected inside an Industrial IoT (IIoT) environment.**

***Index Terms*—5G and beyond networks, distributed signal processing, federated learning, Internet of Things.**

I. Introduction

BEYOND-5G systems are expected to leverage cross-fertilizations between wireless systems, core networking, machine learning (ML), and artificial intelligence (AI) techniques, targeting not only communication and networking tasks but also augmented environmental perception services [1]. The combination of powerful AI tools, e.g., deep neural networks (DNNs), with massive usage of Internet of Things (IoT), is expected to provide advanced services [2] in several domains, such as Industry 4.0 [3], cyber–physical systems (CPSs) [4], and smart mobility [5]. Considering this envisioned landscape, it is of paramount importance to integrate emerging deep learning breakthroughs within future generation wireless networks, characterized by arbitrary distributed connectivity patterns (e.g., mesh, cooperative, peer-to-peer, or spontaneous), along with strict constraints in terms of latency [6], i.e., to support ultrareliable low-latency communications (URLLC) and battery lifetime.

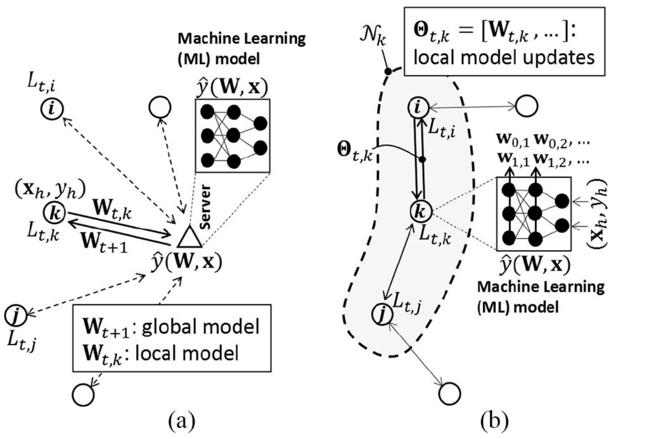
Machine Learning (ML) model
$\hat{y}(\mathbf{W},\mathbf{x})$
$L_{t,i}$
i
$(\mathbf{x}_h, y_h)$
k
$L_{t,k}$
$\mathbf{W}_{t,k}$
$\mathbf{W}_{t+1}$
Server
$\hat{y}(\mathbf{W},\mathbf{x})$
j
$L_{t,j}$
$\mathbf{W}_{t+1}$: global model
$\mathbf{W}_{t,k}$: local model
(a)
$\mathcal{N}_k$
$\mathbf{\Theta}_{t,k} = [\mathbf{W}_{t,k}, \ldots]$: local model updates
$\mathbf{\Theta}_{t,k}$
$L_{t,i}$
$\mathbf{W}_{0,1}\,\mathbf{W}_{0,2}, \ldots$
$\mathbf{W}_{1,1}\,\mathbf{W}_{1,2}, \ldots$
$L_{t,k}$
$(\mathbf{x}_h, y_h)$
$\hat{y}(\mathbf{W},\mathbf{x})$
Machine Learning (ML) model
$L_{t,j}$
(b)

Fig. 1. (a) FL based on centralized fusion of local model (or gradient) updates. (b) Proposed consensus-based FL with distributed fusion over an infrastructureless network. Learning of global model parameters $\mathbf{W}$ from local data examples $(\mathbf{x}_h, y_h)$ is obtained by mutual cooperation between neighbors sharing the local model updates $\Theta_{t,k}$.

Recently, federated optimization, or federated learning (FL) [7], [8] has emerged as a new paradigm in distributed ML setups [9]. The goal of FL systems is to train a shared *global model*, i.e., a neural network (NN) from a federation of participating devices acting as local learners under the coordination of a central server for model aggregation. As shown in Fig. 1(a), FL alternates between a local model computation at each device and a round of communication with a server. Devices, or workers, derive a set of local learning parameters from the available training data, referred to as *local model*. The local model $\mathbf{W}_{t,k}$ at time t and device k is typically obtained via backpropagation and stochastic gradient descent (SGD) [10] methods using local training examples (i.e., data $\mathbf{x}_h$ and labels y_h). The server obtains a global model by fusion of local models and then feeds back such model to the devices. Multiple rounds are repeated until convergence is reached. The objective of FL is thus to build a global model $y = \hat{y}(\mathbf{W};\ \mathbf{x})$ by the cooperation of a number of devices. Model is characterized by parameters $\mathbf{W}$ (i.e., NN weights and biases for each layer) for the output quantity y and the observed (input) data $\mathbf{x}$. Since it decouples the ML stages from the need to send data to the server, FL provides strong privacy advantages compared to conventional centralized learning methods.

Manuscript received November 13, 2019; revised December 19, 2019; accepted December 24, 2019. Date of publication January 6, 2020; date of current version May 12, 2020. This work was supported by the ERA-NET CO-FUND H2020 CHISTERA III Project RadioSense. *(Corresponding author: Stefano Savazzi.)*

Stefano Savazzi and Vittorio Rampa are with Consiglio Nazionale delle Ricerche, IEIIT institute, 20133 Milan, Italy (e-mail: stefano.savazzi@ieiit.cnr.it).

Monica Nicoli is with DIG department, Politecnico di Milano, 20133 Milan, Italy.

Digital Object Identifier 10.1109/JIOT.2020.2964162

A. Decentralized FL and Related Works

Next-generation networks are expected to be underpinned by new forms of decentralized, infrastructureless communication paradigms [11] enabling devices to cooperate directly over device-to-device (D2D) spontaneous connections (e.g., multihop or mesh). These networks are designed to operate—when needed—without the support of a central coordinator, or with limited support for synchronization and signaling. They are typically deployed in mission-critical control applications where edge nodes cannot rely on a remote unit for fast feedback and have to manage the part of the computing tasks locally [12], cooperating with neighbors to self disclose the information. Typical examples are low-latency safety-related services for vehicular [13] or industrial [14] applications. Considering these trends, research activities are now focusing on fully decentralized (i.e., server-less) learning approaches. Optimization of the model running on the devices with privacy constraints is also critical [16] for human-related applications.

To the authors' knowledge, few attempts have been made to address the problem of decentralized FL. In [17] and [18], a gossip protocol is adopted for ML systems. Through sum-weight gossip, local models are propagated over a peer-to-peer network. However, in FL over D2D networks, gossip-based methods cannot be fully used because of medium access control (MAC) and half-duplex constraints, which are ignored in these early approaches. More recently, Guha *et al.* [19] considered an application of distributed learning for medical data centers where several servers collaborate to learn a common model over a fully connected (FC) network. However, network scalability/connectivity issues are not considered at all. In [20], a segmented gossip aggregation is proposed. The global model is split into nonoverlapping subsets and local learners aggregate the segmentation sets from other learners. Having split the model, by introducing *ad hoc* subsets and segment management tasks, the approach is extremely application dependent and not suitable for more general ML contexts. Finally, Lalitha *et al.* [21], [22] proposed a peer-to-peer Bayesian-like approach to iteratively estimate the posterior model distribution. Focus is on convergence speed and load balancing, yet simulations are limited to a few nodes, and the proposed method cannot be easily generalized to NN systems trained by incremental gradient (i.e., SGD) or momentum-based methods.

B. Contributions

This article proposes the application of FL principles to massively dense and fully decentralized networks that do not rely upon a central server coordinating the learning process. As shown in Fig. 1(b), the proposed FL algorithms leverage the mutual cooperation of devices that perform data operations inside the network (in-network) via consensus-based methods [23]. Devices independently perform training steps on their local data set (batches) based on a local objective function, by using SGD and the fused models received from the neighbors. Next, similarly to gossip [17], devices forward the model updates to their one-hop neighborhood for a new consensus step. Unlike the methods in [17]–[22], the proposed approach is general enough to be seamlessly applied to any NN model trained by SGD or momentum methods. In addition, in this article, we investigate the scalability problem for varying NN model layer size, considering large and dense D2D networks with different connectivity graphs. These topics are discussed, for the first time, by focusing on an experimental industrial IoT (IIoT) setting.

This article's contributions are summarized in the following.

1) The federated averaging (FA) algorithm [9], [15] is revisited to allow local learners to implement consensus techniques by exchanging local model updates: consensus also extends existing gossip approaches.
2) A novel class of FL algorithms based on the iterative exchange of *both* model updates *and* gradients is proposed to improve convergence and minimize the number of communication rounds, in exchange for a more intensive use of D2D links and local computing.
3) All presented algorithms are validated over large scale massive networks with intermittent, sporadic, or varying connectivity, focusing in particular on an experimental IIoT setup, and considering both complexity, convergence speed, communication overhead, and average execution time on embedded devices.

This article is organized as follows. Section II reviews the FL problem. Section III proposes two consensus-based algorithms for decentralized FL. Validation of the proposed methods is first addressed in Section IV on a simple network and scenario. Then, in Section V, the validation is extended to a large-scale setup by focusing on a real-world problem in the IIoT domain. Finally, Section VI draws some conclusions and proposes future investigations.

II. FL FOR MODEL OPTIMIZATION

The FL approach defines an incremental algorithm for model optimization over a large population of devices. It belongs to the family of incremental gradient algorithms [26], [29] but, unlike these setups, optimization typically focuses on nonconvex objectives that are commonly found in NN problems. The goal is to learn a global model $\hat{y}(\mathbf{W}; \mathbf{x})$ for inference problems (i.e., classification or regression applications) that transforms the input observation vector $\mathbf{x}$ into the outputs $\hat{y} \in \{y_c\}_{c=1}^{C}$, with model parameters embodied in the matrix $\mathbf{W}$ while C is the output size. Observations, or input data, are stored across K devices connected with a central server that coordinates the learning process. A common, and practical, assumption is that the number of participating devices K is large ($K \gg 1$) and they have intermittent connectivity with the server. The cost of communication is also much higher than local computation, in terms of capacity, latency, and energy consumption [25]. In this article, we will focus specifically on NN models. Therefore, considering an NN of $Q \geq 1$ layers, the model iteratively computes a nonlinear function $f(\cdot)$ of a weighted sum of the input values, namely

$$\hat{y}(\mathbf{W}; \mathbf{x}) = f_Q\left(\mathbf{w}_{0,Q}^T \mathbf{h}_{Q-1} + \mathbf{w}_{1,Q}\right) \tag{1}$$

with $\mathbf{h}_q = f_q(\mathbf{w}_{0,q}^T \mathbf{h}_{q-1} + \mathbf{w}_{1,q})$, $q = 1, \ldots, Q-1$, being the hidden layers and $\mathbf{h}_0 = \mathbf{x}$ the input vector.

The matrix

$$\mathbf{W} = \left[\mathbf{w}_{0,1}^T, \mathbf{w}_{1,1}, \ldots, \mathbf{w}_{0,Q}^T, \mathbf{w}_{1,Q}\right] \tag{2}$$

collects all the parameters of the model, namely, the weights $\mathbf{w}_{0,q} \in \mathbb{R}^{d_1 \times d_2}$ and the biases $\mathbf{w}_{1,q} \in \mathbb{R}^{d_2 \times 1}$ for each defined layer, with d_1 and d_2 the corresponding input and output layer dimensions, respectively.[1] FL applies *independently* to each layer[2] of the network. Therefore, in what follows, optimization focuses on one layer q and the matrix (2) reduces to $\mathbf{W} = [\mathbf{w}_{0,q}^T, \mathbf{w}_{1,q}]$. The parameters of the convolutional layers, namely, input, output, and kernel dimensions, can be easily reshaped to conform with the above general representation.

In FL, it is commonly assumed [7], [8] that a large database of examples is (unevenly) partitioned among the K devices, under nonidentical independent distribution (non-IID) assumptions. Examples are thus organized as the tuples $(\mathbf{x}_h, y_h)$, $h = 1, \ldots, E$, where $\mathbf{x}_h$ represents the data, while y_h are the desired model outputs $\hat{y}$. The set of examples, or training data, available at device k is $\mathcal{E}_k$, where $E_k = |\mathcal{E}_k| \ll E$ is the size of the kth data set under the non-IID assumption. The training data on a given device is thus not representative of the full population distribution. In practical setups (see Section V), data are collected individually by the devices based on their local/partial observations of the given phenomenon.

Unlike incremental gradient algorithms [30], [31], FL of the model $\mathbf{W}$ is applicable to any finite-sum objective $L(\mathbf{W})$ of the general form

$$\min_{\mathbf{W}} L(\mathbf{W}) = \min_{\mathbf{W}} \underbrace{\sum_{k=1}^{K} \frac{E_k}{E} \times L_k(\mathbf{W})}_{L(\mathbf{W})} \tag{3}$$

where $L_k(\mathbf{W})$ is the loss, or cost, associated with the kth device

$$L_k(\mathbf{W}) = \frac{1}{E_k} \sum_{h=1}^{E_k} \ell(\mathbf{x}_h, y_h; \mathbf{W}) \tag{4}$$

and $\ell(\mathbf{x}_h, y_h; \mathbf{W})$ is the loss of the predicted model over the E_k examples $(\mathbf{x}_h, y_h)$ observed by the device k, assuming model parameters $\mathbf{W}$ to hold.

In conventional centralized ML (i.e., learning *without* federation), used here as benchmark, the server collects *all* local training data from the devices and obtains the optimization of model parameters by applying an incremental gradient method over a number of batches from the training data set. For iteration t, the model parameters are thus updated by the server according to

$$\mathbf{W}_{t+1} = \mathbf{W}_t - \mu_s \times \nabla L(\mathbf{W}_t) \tag{5}$$

where μ_s is the SGD step size and $\nabla L(\mathbf{W}_t) = \nabla_{\mathbf{W}_t}[L(\mathbf{W}_t)]$ the gradient of the loss in (3) over the assigned batches and with respect to the model $\mathbf{W}_t$. Backpropagation is used here for gradients computation. The model estimate at convergence is denoted as $\mathbf{W}_\infty = \lim_{t\to\infty} \mathbf{W}_t$.

[1]To simplify the notation, here we assume that the layers have equal input/output size in $\mathbf{W}$, but the model can be generalized to account for different dimensions (see Section V).

[2]Weights and biases are also optimized independently.

Rather than sharing the training data with the server, in FL the model parameters $\mathbf{W}$ are optimized collectively by interconnected devices, acting as local learners. On each round t of communication, the server distributes the current global model $\mathbf{W}_t$ to a subset $\mathcal{S}_t$ of n_t devices. The devices independently update the model $\mathbf{W}_t$ using the gradients (SGD) from *local* training data as

$$\mathbf{W}_{t+1,k} = \mathbf{W}_t - \mu \times \nabla L_{t,k}(\mathbf{W}_t) \tag{6}$$

where $\nabla L_{t,k}(\mathbf{W}_t) = \nabla_{\mathbf{W}_t}[L_{t,k}(\mathbf{W}_t)]$ represents the gradient of the loss (4) observed by the kth device and with respect to the model $\mathbf{W}_t$. Updates $\nabla L_{t,k}$ (6), or local models $\mathbf{W}_{t+1,k}$, are sent back to the server, after quantization, anonymization [7], and compression stages, modeled here by the operator $\mathcal{P}_\Theta$. A global model update is obtained by the server through aggregation according to

$$\mathbf{W}_{t+1} = \mathbf{W}_t - \mu_s \frac{1}{n_t} \sum_{k=1}^{n_t} \frac{E_k}{E} \mathcal{P}_\Theta\left[\nabla L_{t,k}(\mathbf{W}_t)\right]. \tag{7}$$

Convergence toward the centralized approach (5) is achieved if $\lim_{t\to\infty} \mathbf{W}_t = \mathbf{W}_\infty$. Notice that the learning rate μ_s is typically kept smaller [9] compared with centralized learning (5) on large data sets. The aggregation model (7) is referred to as federated averaging (FA) [7], [15]. As far as convergence is concerned, for strongly convex objective $L(\mathbf{W})$ and generic local solvers, the general upper bound on global iteration number N_I is given in [24] and relates both to global (γ_G) and local (γ_L) accuracy according to the equation $N_I = \mathcal{O}(\log[1/(1-\gamma_G)]/\gamma_L)$.

III. Consensus-Based Approach to in-Network FL

The approaches proposed in this section allow the devices to learn the model parameters, solution of (3), by relying *solely* on local cooperation with neighbors, and local in-network (as opposed to centralized) processing. The interaction topology of the network is modeled as a directed graph $\mathcal{G} = (\mathcal{V}, \xi)$ with the set of nodes $\mathcal{V} = \{1, 2, \ldots, K\}$ and edges (links) ξ. As depicted in Fig. 1, the K distributed devices are connected through a decentralized communication architecture based on D2D communications. The neighbor set of device k is denoted as $\mathcal{N}_k = \{i \in V : (i,k) \in \xi\}$, with cardinality $|\mathcal{N}_k|$. Notice that we include node k in the set $\mathcal{N}_k$, while $\mathcal{N}_{\bar{k}} = \mathcal{N}_k \backslash \{k\}$ does not. As introduced in the previous section, each device has a database $\mathcal{E}_k$ of examples $(\mathbf{x}_h, y_h)$ that are used to train a local NN model $\mathbf{W}_{t,k}$ at some time t (epoch). The model maps input features $\mathbf{x}$ into outputs $\hat{y}(\mathbf{W}_{t,k}; \mathbf{x})$ as in (1). A cost function, generally nonconvex, as $L_k(\mathbf{W}_{t,k})$ in (4), is used to optimize the weights $\mathbf{W}_{t,k}$ of the local model.

The proposed FL approaches exploit both adaptive diffusion [31] and consensus tools [23], [27] to optimally leverage the (possibly large) population of federated devices that cooperate for the distributed estimation of the global model $\mathbf{W}$, while retaining the trained data. Convergence is thus obtained if $\forall k$ it is $\lim_{t\to\infty} \mathbf{W}_{t,k} = \mathbf{W}_\infty$. Distributed in-network model optimization must satisfy convergence time constraints, as well as minimize the number of communication rounds. In what follows, we propose two strategies that differ in the way the

Algorithm 1 Consensus-Based FA

```
1: procedure CFA($\mathcal{N}_{\bar{k}}, \epsilon_t, \alpha_{t,i}$)
2:     initialize $\mathbf{W}_{0,k} \leftarrow$ device $k$
3:     for each round $t = 1, 2, \ldots,$ do                ▷ Main loop
4:         receive$\{\mathbf{W}_{t,i}\}_{i \in \mathcal{N}_{\bar{k}}}$                ▷ RX from neighbors
5:         $\boldsymbol{\psi}_{t,k} \leftarrow \mathbf{W}_{t,k}$
6:         for all devices $i \in \mathcal{N}_{\bar{k}}$ do
7:             $\boldsymbol{\psi}_{t,k} \leftarrow \boldsymbol{\psi}_{t,k} + \epsilon_t \alpha_{t,i}(\mathbf{W}_{t,i} - \mathbf{W}_{t,k})$
8:         end for
9:         $\mathbf{W}_{t+1,k} =$ ModelUpdate($\boldsymbol{\psi}_{t,k}$)
10:        send($\mathbf{W}_{t+1,k}$)                ▷ TX to neighbors
11:    end for
12: end procedure
13: procedure ModelUpdate($\boldsymbol{\psi}_{t,k}$)                ▷ Local SGD
14:     $\mathcal{B} \leftarrow$ mini-batches of size $B$
15:     for batch $b \in \mathcal{B}$ do                ▷ Local model update
16:         $\boldsymbol{\psi}_{t,k} \leftarrow \boldsymbol{\psi}_{t,k} - \mu_t \nabla L_{t,k}(\boldsymbol{\psi}_{t,k})$
17:     end for
18:     $\mathbf{W}_{t,k} \leftarrow \boldsymbol{\psi}_{t,k}$
19:     return($\mathbf{W}_{t,k}$)
20: end procedure
```

model updates $\mathbf{W}_{t,k}$ and gradients $\nabla L_{t,k}$ are computed and updated.

A. Consensus-Based Federated Averaging

The first strategy extends the centralized FA and it is described in the pseudocode fragment of Algorithm 1. It is referred to as consensus-based FA (CFA).

After initialization[3] of $\mathbf{W}_{0,k}$ at time $t = 0$, on each communication round $t > 0$, device k sends its model updates $\mathbf{W}_{t,k}$ (once per round) and receives weights from neighbors $\mathbf{W}_{t,i}$, $i \in \mathcal{N}_{\bar{k}}$. Based on received data, the device updates its model $\mathbf{W}_{t,k}$ sequentially to obtain the aggregated model

$$\boldsymbol{\psi}_{t,k} = \mathbf{W}_{t,k} + \epsilon_t \sum_{i \in \mathcal{N}_{\bar{k}}} \alpha_{k,i}\left(\mathbf{W}_{t,i} - \mathbf{W}_{t,k}\right) \tag{8}$$

where ϵ_t is the *consensus step size* and $\alpha_{k,i}$, $i \in \mathcal{N}_{\bar{k}}$, are the mixing weights for the models. Next, gradient update is performed using the aggregated model $\boldsymbol{\psi}_{t,k}$ as

$$\mathbf{W}_{t+1,k} = \boldsymbol{\psi}_{t,k} - \mu_t \nabla L_{t,k}\left(\boldsymbol{\psi}_{t,k}\right) \tag{9}$$

by running SGD over a number of mini-batches of size $B < E_k$. Model aggregation (8) is similar to the sum-weight gossip protocol [17], [18], when setting $\epsilon_t = 1$. However, mixing weights $\alpha_{k,i}$ are used here to combine model innovations, $\{\mathbf{W}_{t,i} - \mathbf{W}_{t,k}\}$, $i \in \mathcal{N}_{\bar{k}}$. In addition, the step size ϵ_t controls the consensus stability.

Inspired by FA approaches (Section II), the mixing weights $\alpha_{k,i}$ are chosen as

$$\alpha_{k,i} = \frac{E_i}{\sum_{i \in \mathcal{N}_{\bar{k}}} E_i}. \tag{10}$$

Other choices are based on weighted consensus strategies [23], where the mixing weights $\alpha_{k,i}$ are adapted on each epoch t based on current validation accuracy or loss metrics. The consensus step size ϵ_t can be chosen as $\epsilon_t \in (0, 1/\Delta)$, where $\Delta = \max_k(\sum_{i \in \mathcal{N}_{\bar{k}}} \alpha_{k,i})$, namely, the maximum degree of the graph $\mathcal{G}$ [28] that models the interaction topology of the network. Notice that the graph $\mathcal{G}$ has adjacency matrix $\mathbf{A} = [a_{k,i}]$, where $a_{k,i} = \alpha_{k,i}$ if $i \in \mathcal{N}_{\bar{k}}$ and $a_{k,i} = 0$ otherwise. Beside consensus step size, it is additionally assumed that the SGD step size μ_t is optimized for convergence: namely, the objective function value $L_{t,k}$ is decreasing with each iteration of gradient descent, or after some threshold. Convergence is further analyzed in Section V with experimental data.

By defining as $\Theta_{t,k}$, the set of parameters to be exchanged among neighbors, CFA requires the iterative exchange of model updates $\mathbf{W}_{t,i}$ $\forall i \in \mathcal{N}_k$, therefore

$$\Theta_{t,k} := \left[\mathbf{W}_{t,k}\right]. \tag{11}$$

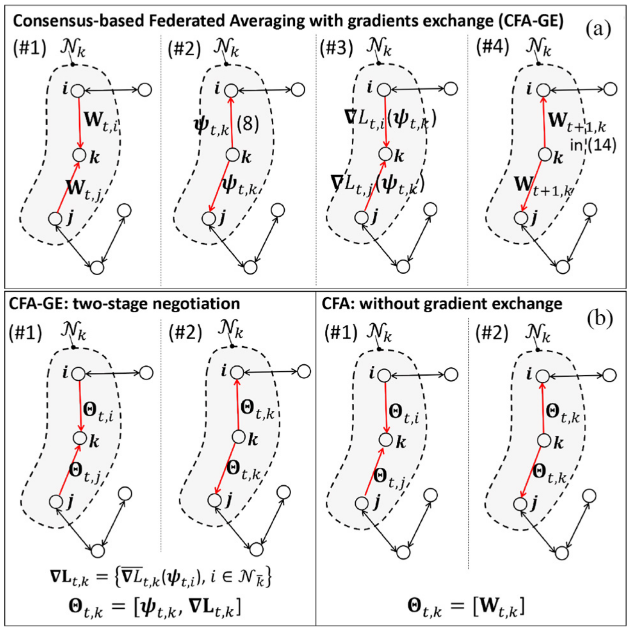
Consensus-based Federated Averaging with gradients exchange (CFA-GE)
(a)
(#1) $\mathcal{N}_k$
(#2) $\mathcal{N}_k$
(#3) $\mathcal{N}_k$
(#4) $\mathcal{N}_k$
i
k
j
$\mathbf{W}_{t,i}$
$\mathbf{W}_{t,j}$
$\boldsymbol{\psi}_{t,k}$ (8)
$\boldsymbol{\psi}_{t,k}$
$\nabla L_{t,i}(\boldsymbol{\psi}_{t,k})$
$\nabla L_{t,j}(\boldsymbol{\psi}_{t,k})$
$\mathbf{W}_{t+1,k}$ in (14)
$\mathbf{W}_{t+1,k}$
CFA-GE: two-stage negotiation
CFA: without gradient exchange
(b)
$\boldsymbol{\Theta}_{t,i}$
$\boldsymbol{\Theta}_{t,j}$
$\boldsymbol{\Theta}_{t,k}$
$\nabla \mathbf{L}_{t,k} = \{\overline{\nabla L}_{t,k}(\boldsymbol{\psi}_{t,i}), i \in \mathcal{N}_{\bar{k}}\}$
$\boldsymbol{\Theta}_{t,k} = [\boldsymbol{\psi}_{t,k}, \nabla \mathbf{L}_{t,k}]$
$\boldsymbol{\Theta}_{t,k} = [\mathbf{W}_{t,k}]$

Fig. 2. (a) CFA-GE. (b) CFA-GE with two-stage negotiation and implementation (left) compared against CFA w/o gradient exchange (right).

B. Consensus-Based Federated Averaging With Gradients Exchange

The second strategy proposes the *joint* exchange of local gradients *and* model updates by following the four-stage iterative procedure illustrated in Fig. 2(a) for epoch t. The new algorithm is referred to as CFA with gradients exchange (CFA-GE). The first stage (step #1) is similar to CFA and obtains $\boldsymbol{\psi}_{t,k}$ by the consensus-based model aggregation in (8). Before using $\boldsymbol{\psi}_{t,k}$ for the local model update, it is fed back to the same neighbors ["negotiation" stage in step #2 of Fig. 2(b)]. Model $\boldsymbol{\psi}_{t,k}$ is then used by the neighbors to compute the gradients

$$\nabla L_{t,i}\left(\boldsymbol{\psi}_{t,k}\right) \; \forall i \in \mathcal{N}_{\bar{k}} \tag{12}$$

using *their* local data. Notice that all gradients are computed over a single batch[4] (or mini-batch) of local data, while the

[3]Each device hosts a model $\mathbf{W}$ of the same architecture and initialized similarly.

[4]Sending multiple gradients (corresponding to mini-batches) is an alternative option, not considered here for bandwidth limitations.

chosen batch/mini-batch can change on consecutive communication rounds. Gradients are sent back to the device k in step #3. Compared with CFA, this step allows every device to exploit additional gradients using neighbor data, and makes the learning much faster. On the device k, the local model is thus updated using the *received* gradients (12) according to

$$\widetilde{\boldsymbol{\psi}}_{t,k} = \boldsymbol{\psi}_{t,k} - \mu_t \sum_{i \in \mathcal{N}_{\bar{k}}} \beta_{k,i} \mathcal{P}_{\Theta}\left[\nabla L_{t,i}\left(\boldsymbol{\psi}_{t,k}\right)\right] \tag{13}$$

where $\beta_{k,i}$ are the mixing weights for the gradients. Finally, as done for CFA in (9), the gradient update is performed using the aggregated model $\widetilde{\boldsymbol{\psi}}_{t,k}$ (13) and *local* data mini-batches

$$\mathbf{W}_{t+1,k} = \widetilde{\boldsymbol{\psi}}_{t,k} - \mu_t \nabla L_{t,k}\left(\widetilde{\boldsymbol{\psi}}_{t,k}\right). \tag{14}$$

To summarize, for each device k, CFA-GE combines the gradients $\nabla L_{t,k}(\boldsymbol{\psi}_{t,k})$ computed over the local data with the gradients $\nabla L_{t,i}(\boldsymbol{\psi}_{t,k})$, $i \in \mathcal{N}_{\bar{k}}$ obtained by the neighbors over their batches. The negotiation stage (13)–(14) is similar to the diffusion strategy proposed in [30] and [31]. In particular, we aggregate the model first (8), then we run one gradient descent round using the received gradients (13), and finally, a number of SGD rounds (14) using local mini-batches. As revealed in Section V, optimization of the mixing weights $\beta_{k,i}$ for the gradients is critical for convergence. Considering that the gradients in (12), obtained from neighbors, are computed over a single batch of data, as opposed to local data mini-batches, a reasonable choice is $\beta_{k,i} > 1$ $\forall i \in \mathcal{N}_{\bar{k}}$. This aspect is further discussed in Section V.

C. Two-Stage Negotiation and Implementation Aspects

Unlike CFA, CFA-GE requires a larger use of the bandwidth and more communication rounds for the synchronous exchange of the gradients. More specifically, it requires a more intensive use of the D2D wireless links for sharing models first during the negotiations (step #2) and then forwarding gradients (step #3). In addition, each device should wait for neighbor gradients before applying any model update. Here, the proposed implementation simplifies the negotiation procedure to improve convergence time (and latency). In particular, it resorts to a two-stage scheme, while, likewise CFA, each device can perform the updates without waiting for a reply from neighbors. Pseudocode is highlighted in Algorithm 2. Communication rounds versus epoch t for CFA-GE are detailed in Fig. 2(b) and compared with CFA. Considering the device k, with straightforward generalization, the following parameters are exchanged with neighbors at epoch t as

$$\Theta_{t,k} := \left[\boldsymbol{\psi}_{t,k}, \nabla \mathbf{L}_{t,k}\right] \tag{15}$$

namely, the model updates (aggregations) $\boldsymbol{\psi}_{t,k}$ and the gradients $\nabla \mathbf{L}_{t,k}$, organized as

$$\nabla \mathbf{L}_{t,k} := \left\{\overline{\nabla L}_{t,k}\left(\boldsymbol{\psi}_{t-1,i}\right) \; \forall i \in \mathcal{N}_{\bar{k}}\right\}. \tag{16}$$

In the proposed two stage implementation, the negotiation step [step #2 in Fig. 2(a)] is not implemented as it requires a synchronous model sharing. Therefore $\forall i \in \mathcal{N}_{\bar{k}}$ the model aggregations $\boldsymbol{\psi}_{t,i}$ are not available by device k at epoch t, or, equivalently, the device k does not wait for such information from the neighbors. The gradients $\nabla L_{t,k}(\boldsymbol{\psi}_{t,i})$ are now *predicted* as $\overline{\nabla L}_{t,k}(\boldsymbol{\psi}_{t-1,i})$ using the past (outdated) models $\boldsymbol{\psi}_{t-1,i}, \boldsymbol{\psi}_{t-2,i}, \ldots,$ from the neighbors. In line with momentum-based techniques (see [32] and also Appendix B), for the predictions $\overline{\nabla L}_{t,k}$ we use a multivariate exponentially weighted moving average (MEWMA) of the past gradients

Algorithm 2 CFA-GE

```
1:  procedure CFA-GE($\mathcal{N}_{\bar{k}}, \epsilon_t, \alpha_{t,i}, \beta_{t,i}$)
2:      initialize $\mathbf{W}_{0,k}, \boldsymbol{\psi}_{1,k}, \nabla L_{1,k}(\boldsymbol{\psi}_{0,k})$
3:      for each round $t = 2, \ldots,$ do                                ▷ Main loop
4:          receive$\{\boldsymbol{\psi}_{t,i}, \overline{\nabla L}_{t,i}(\boldsymbol{\psi}_{t-1,k})\}_{i \in \mathcal{N}_{\bar{k}}}$          ▷ RX
5:          $\boldsymbol{\psi}_{t,k} \leftarrow \mathbf{W}_{t,k}$
6:          for all devices $i \in \mathcal{N}_{\bar{k}}$ do
7:              $\boldsymbol{\psi}_{t,k} \leftarrow \boldsymbol{\psi}_{t,k} + \epsilon_t \alpha_{t,i}(\boldsymbol{\psi}_{t,i} - \mathbf{W}_{t,k})$
8:              compute $\nabla L_{t+1,k}(\boldsymbol{\psi}_{t,i})$                    ▷ gradients
9:              $\overline{\nabla L}_{t+1,k} \leftarrow$ in (17)                      ▷ MEWMA update
10:         end for
11:         $\widetilde{\boldsymbol{\psi}}_{t,k} \leftarrow \boldsymbol{\psi}_{t,k}$
12:         for all devices $i \in \mathcal{N}_{\bar{k}}$ do
13:             $\widetilde{\boldsymbol{\psi}}_{t,k} \leftarrow \widetilde{\boldsymbol{\psi}}_{t,k} - \mu_t \beta_{t,i} \overline{\nabla L}_{t,i}(\boldsymbol{\psi}_{t-1,k})$
14:         end for
15:         $\mathbf{W}_{t+1,k} \leftarrow$ ModelUpdate($\widetilde{\boldsymbol{\psi}}_{t,k}$)
16:         $\boldsymbol{\psi}_{t+1,k} \leftarrow \boldsymbol{\psi}_{t,k}$
17:         $\nabla \mathbf{L}_{t+1,k} := \{\overline{\nabla L}_{t+1,k} \; \forall i \in \mathcal{N}_{\bar{k}}\}$.
18:         send($\boldsymbol{\psi}_{t+1,k}, \nabla \mathbf{L}_{t+1,k}$)                 ▷ TX to neighbors
19:     end for
20: end procedure
```

$$\overline{\nabla L}_{t,k}\left(\boldsymbol{\psi}_{t-1,i}\right) = \varrho \nabla L_{t,k}\left(\boldsymbol{\psi}_{t-1,i}\right) + (1 - \varrho)\overline{\nabla L}_{t-1,k} \tag{17}$$

ruled by the hyperparameter $0 < \varrho \leq 1$. Setting $\varrho = 1$, the gradient is estimated using the last available model $(\boldsymbol{\psi}_{t-1,i})$: $\overline{\nabla L}_{t,k}(\boldsymbol{\psi}_{t-1,i}) = \nabla L_{t,k}(\boldsymbol{\psi}_{t-1,i})$. A smaller value $\varrho < 1$ introduces a memory $(1 - \varrho)\overline{\nabla L}_{t-1,k}$ with $\overline{\nabla L}_{t-1,k} = \overline{\nabla L}_{t-1,k}(\boldsymbol{\psi}_{t-2,i}, \ldots)$ depending on the past models $\boldsymbol{\psi}_{t-2,i}, \ldots$ This is shown, in Section V, to be beneficial on real data.

Assuming that the device k is able to correctly receive and decode the messages from the neighbors $\Theta_{t,i} = [\boldsymbol{\psi}_{t,i}, \nabla \mathbf{L}_{t,i}]$ $\forall i \in \mathcal{N}_{\bar{k}}$ at epoch t, the model aggregation step changes from (8) to

$$\boldsymbol{\psi}_{t,k} = \mathbf{W}_{t,k} + \epsilon_t \sum_{i \in \mathcal{N}_{\bar{k}}} \alpha_{k,i}\left(\boldsymbol{\psi}_{t,i} - \mathbf{W}_{t,k}\right) \tag{18}$$

while the model update step using the *received* gradients is now

$$\widetilde{\boldsymbol{\psi}}_{t,k} = \boldsymbol{\psi}_{t,k} - \mu_t \sum_{i \in \mathcal{N}_{\bar{k}}} \beta_{k,i} \mathcal{P}_{\Theta}\left[\nabla L_{t,i}\left(\boldsymbol{\psi}_{t-1,k}\right)\right] \tag{19}$$

and replaces (13). Finally, a gradient update on local data is done as in (14). Notice that Algorithm 2 implements (19) by running one gradient descent round per received gradient (lines 12–14) to allow for asynchronous updates. In Appendix B, we discuss the application of CFA and CFA-GE to advanced SGD strategies designed to leverage momentum information [10], [32].

D. Communication Overhead and Complexity Analysis

With respect to FA, the proposed decentralized algorithms take some load off of the server, at the cost of additional in-network operations and increased D2D communication overhead. Overhead is quantified here for both CFA and CFA-GE in terms of the size of the parameters $\Theta_{t,k}$ that need to be exchanged among neighbors. CFA extends FA and, similarly, requires each node to exchange only local model updates at most once per round. The overhead, or the size of $\Theta_{t,k}$, thus corresponds to the model size (11). For a generic DNN model of Q layers, the model $\mathbf{W}_{t,k}$ size can be approximated in the order of $\mathcal{O}(d_1 d_2 Q) \ll E$. This is several orders of magnitude lower than the size of the input training data, in typical ML and deep ML problems. As in (15), CFA-GE requires the exchange of local model aggregations $\boldsymbol{\psi}_{t,k}$ and one gradient $\overline{\nabla L}_{t,k}(\boldsymbol{\psi}_{t-1,i})$ per neighbor $\forall i \in \mathcal{N}_{\bar{k}}$. Overhead now scales with $\mathcal{O}(d_1 d_2 Q |\mathcal{N}_k|)$, where $|\mathcal{N}_k| = |\mathcal{N}_{\bar{k}}| + 1$. This is still considerably lower than the training data set size, provided that the number of participating neighbors is limited. In the examples of Section V, we show that $|\mathcal{N}_{\bar{k}}| = 2$ neighbors are sufficient, in practice, to achieve convergence: notice that the number of active neighbors is also typically small to avoid traffic issues [37]. Finally, quantization $\mathcal{P}_{\Theta}[\,\cdot\,]$ of the parameters can be also applied to limit the transmission payload, with the side effect to improve also global model generalization [38].

Besides overhead, CFA and CFA-GE computational complexity scales with the global model size and it is ruled by the number of local SGD rounds. However, unlike FA, model aggregations *and* local SGD are both implemented on the device. With respect to CFA, CFA-GE computes up to $|\mathcal{N}_{\bar{k}}|$ additional gradients $\overline{\nabla L}_{t,k}(\boldsymbol{\psi}_{t-1,i})$ using neighbor models $\boldsymbol{\psi}_{t-1,i}$ and up to $|\mathcal{N}_{\bar{k}}|$ additional gradient descent rounds (19) for local model update using the neighbor gradients. A quantitative evaluation of the overhead and the execution time of local computations are proposed in Section V by comparing FA, CFA, and CFA-GE using real data and low-power system on chip (SoC) devices.

Considering now networking aspects, the cost of a D2D communication is much lower than the cost of a server connection, typically long range. D2D links cover shorter ranges and require lower transmit power: communication cost is thus ruled by the energy spent during receiving operations (radio wake-up, synchronization, and decoding). Besides, in large-scale and massive IIoT networks, sending model updates to the server, as done in conventional FA, might need several D2D communication rounds as relaying information via neighbor devices. D2D communications can serve as an underlay to the infrastructure (server) network and can thus exploit the same radio resources. Such two-tier networks are a key concept in the next generation IoT and 5G [39] scenarios.

Finally, optimal trading between in-network and server-side operations is also possible by alternating rounds of FA with rounds of in-network consensus (CFA or CFA-GE). This corresponds to a real-world scenario where communication with the server is available, but intermittent, sporadic, unreliable, or too costly. During initialization, i.e., at time $t = t_0$, devices might use the last available global model received from the server, $\mathbf{W}_{t_0,k} = \mathbf{W}_{N_s}$, after N_s communication rounds of the previous FA phase, and obtain a local update via SGD: $\mathbf{W}_{t+1,k} = \mathbf{W}_{N_s} - \mu_t \nabla L_{t,k}(\mathbf{W}_{N_s})$. This is fed back to neighbors to start CFA or CFA-GE iterations.

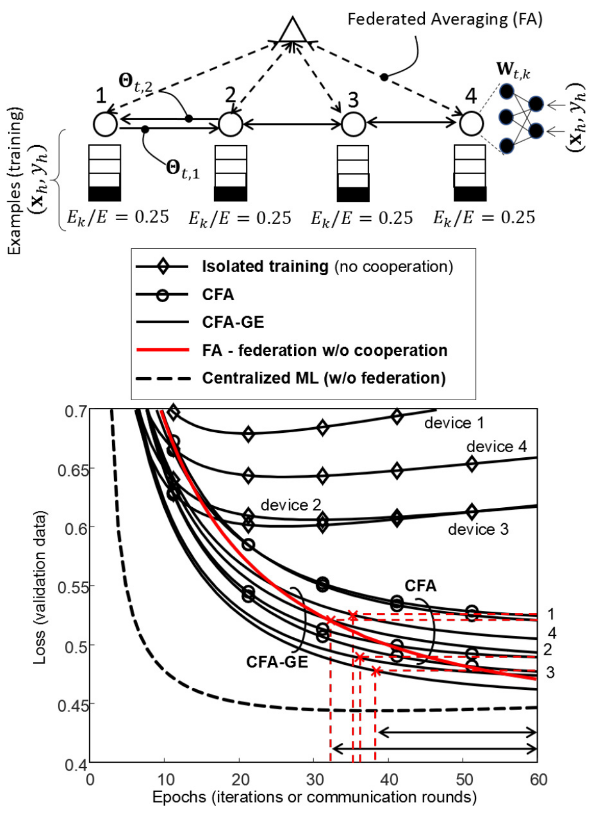

Fig. 3. Comparison of FL methods over a multihop wireless network of $K = 4$ devices. Validation loss versus iterations over the full MNIST data set for all devices: CFA (circle markers), CFA-GE (solid lines without markers), FA (red line), isolated model training (diamond markers), and centralized ML without federation (dashed line). Iterations correspond to *epochs* when running inside the server, or *communication rounds* when running consensus or FA.

IV. Consensus-Based FL: Introductory Example

In this section, we give an introductory example of consensus-based FL approaches comparing their performance to conventional FL methods. We resort here to a network of $K = 4$ wireless devices communicating via multihop as depicted in Fig. 3 without any central coordination. Although simple, the proposed topology is still useful in practice to validate the performance of FL under the assumption that no device has direct (i.e., single hop) connection with all nodes in the network. More practical usage scenarios are considered in Section V. Without affecting generality, the devices collaboratively learn a global model $\hat{y}(\mathbf{W}; \mathbf{x})$ that is simplified here as a NN model with only one FC layer ($Q = 1$)

$$\hat{y}(\mathbf{W}; \mathbf{x}) = f_1\left(\mathbf{w}_{0,1}^T \mathbf{x} + \mathbf{w}_{1,1}\right), \mathbf{W} = \left[\mathbf{w}_{0,1}^T, \mathbf{w}_{1,1}\right]. \quad (20)$$

Considering the 4-node network layout, the neighbor sets consist of $\mathcal{N}_{\bar{1}} = \{2\}$, $\mathcal{N}_{\bar{2}} = \{1, 3\}$, $\mathcal{N}_{\bar{3}} = \{2, 4\}$, and $\mathcal{N}_{\bar{4}} = \{3\}$. Each kth device has a database of E_k local training data, $\mathcal{E}_k = \{(\mathbf{x}_h, y_h)\}_{h=1}^{E_k}$, that are here taken from the Modified National Institute of Standards and Technology (MNIST)

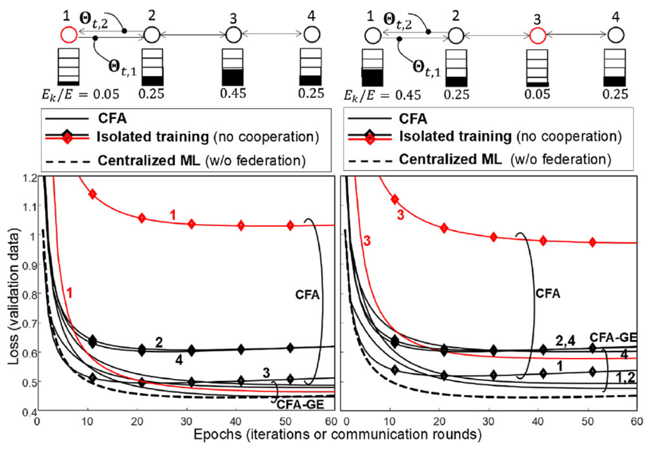

Fig. 4. Effect of non-IID unbalanced training data over device $k = 1$ and $k = 3$ (red lines) of a multihop wireless network composed of $K = 4$ devices. Validation loss over the full MNIST data set versus epochs (or consensus iterations). Comparison between CFA (solid lines), isolated model training (diamond markers), and centralized ML without federation (dashed line) is also presented. Non-IID data distribution is shown visually on top, for each case.

image database [40] of handwritten digits. Output labels y_h take $C = 10$ different values (from digit 0 to 9), model inputs $\mathbf{x}$ have size $d_1 = 784$ (each image is represented by 28×28 grayscale pixels), while outputs $\hat{y}$ have dimension $d_2 = C = 10$. In Fig. 3, each device obtains the same number of training data ($E_k = 400$ images) taken randomly (IID) from the database consisting of $E = 1600$ images. Non-IID data distribution is investigated in Fig. 4.

We assume that each device has prior knowledge of the model (20) structure at the initial stage ($t = 0$), namely, the input/output size (d_1, d_2) and the nonlinear activation $f_1(\cdot)$. Moreover, each of the $K = 4$ local models starts from the same random initialization $\mathbf{W}_{0,k}$ for $t = 0$ [15]. Every new epoch $t > 0$, the devices perform consensus iterations using the model parameters received from the available neighbors during the previous epoch $t - 1$. Local model updates for CFA (9) and CFA-GE (14) use the cross-entropy loss for gradient computation

$$L_{t,k} = -\sum_h y_h \log\left[\hat{y}(\mathbf{W}_{t,k}; \mathbf{x}_h)\right] \tag{21}$$

where the sum is computed over mini-batches of size $B = 5$. The devices thus make one training pass over their local data set consisting of $E_k/B = 80$ mini-batches. For CFA, we choose $\epsilon_t = 1$, $\mu_t = 0.025$, and mixing parameters as in (10). For CFA-GE, the mixing parameters for gradients (13) are selected as $\mu_t \beta_{t,k} = 0.025$ and $\mu_t \beta_{t,i} = 0.2 \; \forall i \in \mathcal{N}_{\bar{k}}$, while the MEWMA hyperparameter is set to $\varrho = 0.99$.

On every epoch t, performance is analyzed in terms of validation loss (21) for all $K = 4$ models. For testing, we considered the full MNIST validation data set $(\mathbf{x}_{h,\text{val}}, y_{h,\text{val}})$ consisting of 60.000 images. The loss $L_{t,k}^{(\text{val})} = -\sum_h y_{h,\text{val}} \log[\hat{y}(\mathbf{W}_{t,k}; \mathbf{x}_{h,\text{val}})]$ decreases over consecutive epochs as far as the model updates $\mathbf{W}_{t,k}$ converge to the *true* global model $\mathbf{W}_\infty$.

In Figs. 3 and 4, we validate the performances of the CFA algorithms in case of uniform (Fig. 3) and uneven (Fig. 4) data distribution among the devices. More specifically, Fig. 3 compares CFA and CFA-GE, with CFA-GE using the two-stage negotiation algorithm of Section III-C and starting[5] at epoch $t = 3$. On the other hand, in Fig. 4, we consider the general case where the data are unevenly distributed, while partitioning among devices is also non-IID. Herein, we compare two cases. In the first one, device 1 (Fig. 4 on the left) is located at the edge of the network and connected to one neighbor only. It obtains $E_k = 80$ images from only 6 of the available C classes, namely, the 5% of the training database of E images. Device 3, connected with two neighbors, retains a larger database ($E_k = 720$ images, 45% of the training database). In the second case (on the right), the situation is reversed. As expected, compared with the first case, convergence is more penalized in the second case, although CFA running on device 3 (red lines) can still converge. As shown in Fig. 3, CFA-GE (solid lines without markers) further reduces the loss, compared with CFA (circle markers). Effect of an unbalanced database for CFA-GE is also considered in Section V.

FL and consensus schemes have been implemented using the TensorFlow library [33], while real-time D2D connectivity is simulated by a Monte Carlo approach. All simulations are running for a maximum of 60 epochs. Besides the proposed consensus strategies, validation loss is also computed for three different scenarios. The first one is labeled as *isolated training* and it is evaluated in Fig. 3 for IID and in Fig. 4 for non-IID data. In this scenario, $K = 4$ models are trained without any cooperation from neighbors (or server) by using locally trained data only. This use case is useful to highlight the benefits of mutual cooperation that are significant after epoch $t = 9$ for IID and after $t = 3$ epochs for non-IID, according to the considered network layout. Notice that isolated training is also limited by overfitting effects after iteration $t = 30$, as clearly observable in Figs. 3 and 4, since local/isolated model optimization is based only on few training images, compared with the validation database of 60.000 images. Consensus and mutual cooperation among devices thus prevent such overfitting. The second scenario *centralized ML without federation* (dashed lines in Figs. 3 and 4) corresponds to (5) and gives the validation loss obtained when all nodes are sending *all* their locally trained data directly to the server. It serves as a benchmark for convergence analysis as provides the optimal parameter set $\mathbf{W}$ considering $E = 1.600$ images for training. Notice that the CFA-GE method closely approaches the optimal parameter set and converges faster than CFA. The third scenario implements the *FA strategy* (see Section II) that relies on server coordination, while cooperation among devices through D2D links is not enabled. As depicted in Fig. 3, the convergence of the FA validation loss is similar to those of devices 2 and 3, although convergence speed is slightly faster after epoch $t = 55$. In fact, for the considered network layout, devices 2 and 3 can be considered a good replacement of the server, being directly connected with most of the devices. In the next section, we consider a more complex device deployment in an IIoT challenging scenario.

[5]At initial epochs $t = 0, 1, 2$, we use the 4-stage negotiation algorithm, described in Section III-B.

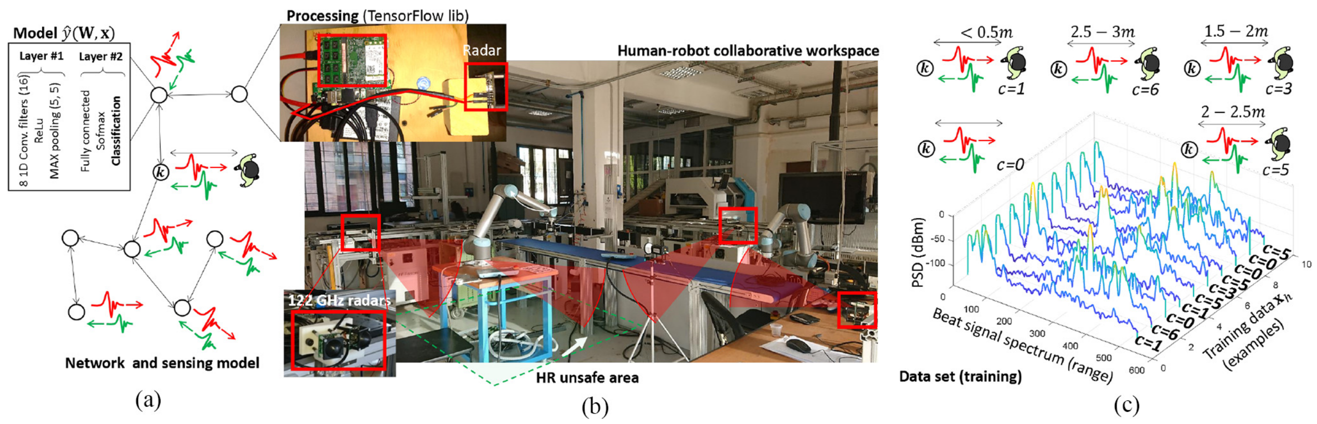

Fig. 5. (a) Experimental setup: network and sensing model for in-network FL with convolutional neural network (CNN, top-left corner) examples whose parameters are shown in Table I. (b) Industrial scenario (CNR-STIIMA de-manufacturing pilot plant) and deployed radars. (c) Examples $\mathbf{x}_h$ of measured beat signal spectrum (512 point FFT) for selected classes ($c = 0, 1, 3, 5, 6$).

V. Validation in Experimental IIoT Scenario

The proposed in-network FL approaches of Section IV are validated here on a real-world IIoT use case. Data are partitioned over IIoT devices and D2D connectivity [14] is used here as a replacement to centralized communication infrastructure [34]. As depicted in Fig. 5, the reference scenario consists of a large-scale and dense network [35] of autonomous IIoT devices that are sensing their surroundings using frequency-modulated continuous-wave (FMCW) radars [45] working in the 122-GHz (sub-Thz) band. Radars in the mmWave (or sub-THz) bands are very effective in robotic cells—as in Fig. 5(b) for environment/obstacle detection [36], velocity/distance measurement, and virtual reality applications [43]. In addition, mmWave radios have been also considered as candidates for 5G new radio (NR) allocation. Thus, they represent promising solutions toward the convergence of dense communications and advanced sensing technologies [3].

In the proposed setup, the above-cited devices are employed to monitor a shared industrial workspace during human–robot collaboration (HRC) tasks to detect and track the position of the human operators (i.e., the range distance from the individuals) that are moving nearby a robotic manipulator inside a fenceless space [42]. In industrial shared workplaces, measuring positions and distance are mandatory to enforce a worker protection policy, to implement collision avoidance, reduction of speed, anticipating contacts of limited entity, etc. In addition, it is highly desirable that operators are set free from wearable devices to generate location information [3]. Tracking of body movements must also not depend on active human involvement. For a static background, the problem of passive body detection and ranging can be solved via background subtraction methods, and ML tools (see [44] and references therein). The presence of the robot, often characterized by a massive metallic size, that moves inside the shared workplace, poses additional remarkable challenges in ranging and positioning, because robots induce large, nonstationary, and fast RF perturbation effects [42].

The radars collect a large amount of data, that cannot be shipped back to the server for training and inference, due to the latency constraints imposed by the worker safety policies. In addition, direct communication with the server is available but reserved to monitor the robot activities [42] (and replanning robotic tasks in case of dangerous situations) and should not be used for data distribution. Therefore, to solve the scalability challenge while addressing latency, reliability, and bandwidth efficiency, we let the devices perform model training without any server coordination but using only mutual cooperation with neighbors. We thus adopt the proposed in-network FL algorithms relying solely on local model exchanges over the D2D active links.

In what follows, we first describe the data set and the ML model $\hat{y}(\mathbf{W};\mathbf{x})$ adopted for body motion recognition. Next, we investigate the convergence properties of CFA and CFA-GE solutions, namely, the required number of communication rounds (i.e., latency) for varying connectivity layouts, network size, and hyperparameters choices, such as mixing weights and step sizes. Finally, we provide a quantitative evaluation of the communication overhead and of the local computational complexity comparing all proposed algorithms.

A. Data Collection and Processing

In the proposed setup, the radar (see [43] for a review) transmitting antennas radiate a sweeped modulated waveform [45] with a bandwidth equal to 6-GHz, carrier frequency 119-GHz, and ramp (pulse) duration set to $T = 1$ ms. The radar echoes, reflected by moving objects are mixed at the receiver with the transmitted signal to obtain the beat signal. Beat signals are then converted in the frequency domain (i.e., beat signal spectrum) by using a 512-point fast Fourier transform (FFT) and averaged over ten consecutive frames (i.e., frequency sweeps or ramps). FFT samples are used as model inputs $\mathbf{x}_h$ and serve as training data collected by the individual devices. The network of radars is designed to discriminate body movements from robots and, in turn, to detect the distance of the worker from the robot with the purpose of identifying potentially unsafe conditions [36]. The ML model is here trained to classify $C = 8$ potential HR collaborative situations characterized by different HR distances corresponding to safe or unsafe conditions. In particular, class $c = 0$ (model output $\hat{y} = y_0$)

TABLE I
NN MODELS AND TRAINABLE PARAMETERS $\mathbf{W}$ (WEIGHTS AND BIASES) FOR $C = 8$ CLASSES

NN model	CNN	2-NN
	8 1D conv. (16 taps) $\rightarrow$ ReLu $\rightarrow$ MaxPool (5, 5) $\rightarrow$ FC($168 \times C$) $\rightarrow$ Softmax	FC (512×32) $\rightarrow$ ReLu $\rightarrow$ FC($32 \times C$) $\rightarrow$ Softmax
Layer $q = 1$	$\mathbf{w}_{0,1}$: $d_1 = 16$, $d_2 = 8$	$\mathbf{w}_{0,1}$: $d_1 = 512$, $d_2 = 32$
	$\mathbf{w}_{1,1}$: $d_1 = 8$	$\mathbf{w}_{1,1}$: $d_1 = 32$
Layer $q = 2$	$\mathbf{w}_{0,2}$: $d_1 = 168$, $d_2 = C$	$\mathbf{w}_{0,2}$: $d_1 = 32$, $d_2 = C$
	$\mathbf{w}_{1,2}$: $d_1 = C$	$\mathbf{w}_{1,2}$: $d_1 = C$

corresponds to the robot and the worker cooperating at a safe distance (distance $\geq$ 3.5 m), class $c = 1$ ($\hat{y} = y_1$) identifies the human operator as working close by the robot, at distance $<$ 0.5 m. The remaining classes are: $c = 2$ (0.5 $\leq$ distance $<$ 1 m), $c = 3$ (1 $\leq$ distance $<$ 1.5 m), $c = 4$ (1.5 $\leq$ distance $<$ 2 m), $c = 5$ (2 $\leq$ distance $<$ 2.5 m), $c = 6$ (2.5 $\leq$ distance $<$ 3 m), and $c = 7$ (3 $\leq$ distance $<$ 3.5 m). The FFT range measurements (i.e., beat signal spectrum) and the corresponding true labels in Fig. 5(c), are collected independently by the individual devices and stored locally. During the initial FL stage, each device independently obtains $E_k = 25$ FFT range measurements. Data distribution is also non-IID: in other words, most of the devices have local examples only for a (random) subset of the $C = 8$ classes of the global model. However, we assume that there are sufficient examples for each class considering the data stored on all devices. Local data sets correspond to the 1% of the full training database. Mini-batches for local gradients have size equal to $B = 5$, training passes thus consist of $E_k/B = 5$ mini-batches, for fast model update. On the contrary, validation data consists of $E = 16.000$ range measurements collected inside the industrial plant.

Unlike the previous section, we now choose an ML global model characterized by an NN with $Q = 2$ trainable layers. In particular, two networks are considered with hyperparameters and corresponding dimensions for weights and biases $\mathbf{W} = [\mathbf{w}_{0,1}^T, \mathbf{w}_{1,1}, \mathbf{w}_{0,2}^T, \mathbf{w}_{1,2}]$ that are detailed in Table I. The first convolutional NN model (CNN) consists of a 1-D convolutional layer (8 filters with 16 taps) followed by max-pooling (non-trainable, size 5, and stride 5) and a FC layer of dimension $168 \times C$. The second model (2NN) replaces the convolutional layer with an FC layer of 32 hidden nodes (dimension 512×32) followed by a ReLu layer and a second FC layer of dimension $32 \times C$. The examples are useful to assess the convergence properties of the proposed distributed strategies for different layer types, dimensions, and number of trainable parameters. As before, we further assume that, during the initial stage, each device has knowledge of the ML global model structure (see layers and dimensions in Table I). At each new communication round, model parameters for each layer are multiplexed and propagated simultaneously by using a time-division multiple access (TDMA) scheme [14].

TABLE II
OPTIMIZED HYPERPARAMETERS FOR CFA AND CFA-GE

Configuration (1)	Configuration (2)	Configuration (3)
$K < 15$	$K \in [15, 50]$	$K > 50$
$\lvert\mathcal{N}_{\bar{k}}\rvert \leq 6$	$\lvert\mathcal{N}_{\bar{k}}\rvert \in [2, 6]$	$\lvert\mathcal{N}_{\bar{k}}\rvert = 2$
CFA		
$\epsilon_t = 1$	$\epsilon_t = 0.5$	$\epsilon_t = 0.5$
$\mu_t = 0.025$	$\mu_t = 0.025$	$\mu_t = 0.025$
$\alpha_{k,i}$ in (10)	$\alpha_{k,i}$ in (10)	$\alpha_{k,i}$ in (10)
CFA-GE		
$\mu_t \beta_{k,i} \leq 0.15$	$\mu_t \beta_{k,i} \in [.1, .15]$	$\mu_t \beta_{k,i} \leq 0.1$
$\varrho = 0.99$	$\varrho = 0.95 \div 0.99$	$\varrho = 0.9 \div 0.95$
(MEWMA)	(MEWMA)	(MEWMA)

FL has been simulated on a virtual environment but using real data from the plant. This virtual environment creates an arbitrary number of virtual devices, each configured to process an assigned training data set and exchanging parameters $\Theta_{t,k}$ that are saved in real time on temporary cache files. Files may be saved on RAM disks to speed up the simulation time. The software is written in Python and uses TensorFlow and multiprocessing modules: simplified configurations for testing both CFA and CFA-GE setups are also provided in the repository [46]. The code script examples are available as open source and show the application of CFA and CFA-GE for different NN models. Hyperparameters, such as learning rates for weights $\alpha_{k,i}$, gradients $\mu_t \beta_{k,i}$, number of neighbors $\mathcal{N}_{\bar{k}}$, and ϱ in (17) are fully configurable. The data sets obtained in the scenario of Fig. 5(b) are also available in the same repository. Finally, examples have been provided for implementation and analysis of execution time on low-power devices (Section V-C). The current optimization toolkit does not simulate, or account for, packet losses during communication: this is considered as negligible for short-range connections. However, the network and connectivity can be time varying and arbitrarily defined.

B. Gradient Exchange Optimization for NN

In what follows, FL is verified by varying the number of devices $K = 30 \div 80$ and the number of neighbors $\lvert\mathcal{N}_{\bar{k}}\rvert = 2 \div 10$ to test different D2D connectivity layouts. In Fig. 6, we validate the consensus-based FL tool, for both CNN and 2NN models, over networks with $K = 30$ and $K = 80$. To simplify the analysis of different connectivity scenarios, the network is simulated as k-regular (i.e., all network devices have the same number of neighbors, or degree) while we verify realistic topologies characterized by $\lvert\mathcal{N}_{\bar{k}}\rvert = 2, 4, 6, 10$ neighbors per node. First, in Fig. 6, we compare decentralized CFA and CFA-GE with FA and conventional centralized ML without federation in (5). The chosen optimization hyperparameters are summarized in Table II. For all FL cases (CFA, CFA-GE, and FA), we plot the validation loss versus communication rounds (i.e., epochs) averaged over all K devices. For centralized ML (dashed lines), validation loss is analyzed over epochs now running inside the server. The CFA plots (circle markers) approach slowly the curve corresponding to FA and centralized ML, while performance improves in dense networks (dotted lines). CFA-GE curves (solid and dotted lines without markers) are comparable with FA, and converge after $50-60$ communication rounds. Use of $\lvert\mathcal{N}_{\bar{k}}\rvert = 2$

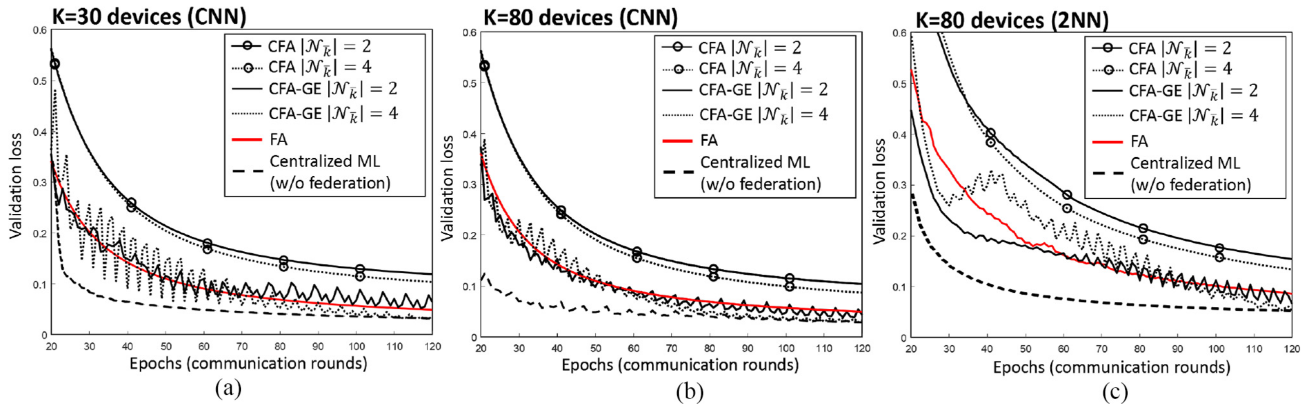

Fig. 6. (a) FL for the CNN model with $K = 30$, (b) $K = 80$ devices, and (c) 2NN model with $K = 80$ devices. The network is characterized by $|\mathcal{N}_{\bar{k}}| = 2$ (solid lines) and $|\mathcal{N}_{\bar{k}}| = 4$ (dotted lines) neighbors per node. Comparative analysis of CFA, CFA-GE, FA (red lines), and centralized ML, i.e., learning w/o federation (dashed lines). CNN and 2NN parameters are described in Table I.

TABLE III
COMMUNICATION ROUNDS (EPOCHS t) FOR TARGET VALIDATION LOSS: $L_{t,k}^{(\mathrm{val})} \leq 0.5\ \forall k$. MIN. AND MAX. EPOCHS OVER $K = 80$ DEVICES FOR CNN AND 2NN. OPTIMIZED PARAMETERS (BOLD) ARE SHOWN AS WELL

	Layers	CNN ($L_{t,k}^{(val)} \leq 0.5$)		2NN ($L_{t,k}^{(val)} \leq 0.5$)	
$\lvert\mathcal{N}_{\bar{k}}\rvert$	($\mathbf{W}$)	$\mu_t\beta_{k,i}$	Epochs (t) (min | max)	$\mu_t\beta_{k,i}$	Epochs (t) (min | max)
2	$q = 1$	**0.2**	9 | **21**	0.05	11 | 51
	$q = 2$	**0.15**		0.1	
	$q = 1$	0.15	10 | 26	**0.1**	12 | **23**
	$q = 2$	0.2		**0.05**	
6	$q = 1$	**0.15**	8 | **18**	0.025	17 | 28
	$q = 2$	**0.1**		0.05	
	$q = 1$	0.1	12 | 23	**0.05**	11 | **19**
	$q = 2$	0.15		**0.025**	
10	$q = 1$	**0.05**	7 | **14**	0.025	15 | 23
	$q = 2$	**0.025**		0.025	
	$q = 1$	0.025	11 | **17**	**0.05**	10 | **17**
	$q = 2$	0.05		**0.025**	

neighbors (solid lines) is sufficient to approach FA performances. Increasing the number of neighbors to $|\mathcal{N}_{\bar{k}}| = 4$ (dotted lines) makes the validation loss comparable with the centralized ML without federation. Running local SGD on received gradients as in (19) causes some fluctuations of the validation loss as approaching convergence. Fluctuations are due to the (large) step size $\mu_t\beta_{k,i}$ used to combine the gradients every communication round: learning rate adaptation techniques [10] can be applied for fine-tuning. Considering the 2NN model, validation loss is larger for all cases as the result of the larger number of model parameters to train, compared with CNN. CFA-GE is still comparable with FA mostly after 70 rounds and converges toward centralized ML after 110 rounds. In all cases, $|\mathcal{N}_{\bar{k}}| = 2$ neighbors are sufficient to approach FA results. More neighbors provide performance improvements mostly in small networks ($K = 30$ devices), while it is still useful to match centralized ML performances.

In Fig. 7, we consider the CFA-GE method and analyze more deeply the effect of the hyperparameter choice on convergence, for $K = 80$ devices and varying network degrees $|\mathcal{N}_{\bar{k}}|$. The first case ($|\mathcal{N}_{\bar{k}}| = 2$) is representative of a multihop wireless network; networks with larger degrees ($|\mathcal{N}_{\bar{k}}| = 6$, $|\mathcal{N}_{\bar{k}}| = 10$) are useful to verify the performance of FL over denser networks. Line plots with bars in Fig. 7 are used to graphically represent the variability of the validation loss observed by the devices. We analyze the learning rate ($\mu_t\beta_{k,i}$) used to combine the gradients received from the neighbors in (19). Other hyperparameters are selected as in Table II. As expected, increasing the network degree helps convergence and makes the validation loss to decrease faster since less communication rounds are required. However, while for $|\mathcal{N}_{\bar{k}}| = 2$ degree networks the learning rates $\mu_t\beta_{k,i}$ can be chosen arbitrarily in the range $\mu_t\beta_{k,i} = 0.1 \div 0.2$ without affecting performance, denser networks, i.e., with large degree $|\mathcal{N}_{\bar{k}}| = 10$, require the optimization of the learning rate: smaller rates $\mu_t\beta_{k,i} \leq 0.1$ improve convergence for $|\mathcal{N}_{\bar{k}}| = 6$ and $|\mathcal{N}_{\bar{k}}| = 10$.

In Table III, we analyze the latency of the FL process that is measured here in terms of number of communication rounds. CFA-GE is considered in detail, while performance of CFA can be inferred from Fig. 6. The Table III reports the number (t) of communication rounds (or epochs) that are required to achieve a target validation loss for all devices, such that $L_{t,k}^{(\mathrm{val})} \leq 0.5\ \forall k$. For the considered case, the chosen validation loss of 0.5 corresponds to a (global) accuracy of $\gamma_G = 0.9$. Focusing on CNN layers, a network with $|\mathcal{N}_{\bar{k}}| = 2$ neighbors per device requires a max of 21 communication rounds (and a minimum of 9) to achieve a target loss of $L_{t,k}^{(\mathrm{val})} \leq 0.5$. This is in line with the theoretical bound [24] $\log[1/(1-\gamma_G)]/\gamma_L = 15$ for local accuracy $\gamma_L \simeq 0.2$ (obtained by isolated training). Considering FA (not shown in the table), the number of required rounds ranges from 7 to 16, and it is again comparable with decentralized optimization. Increasing the number of neighbors to $|\mathcal{N}_{\bar{k}}| = 6$, the required communication rounds reduce to 18 and to 14 for $|\mathcal{N}_{\bar{k}}| = 10$. For 2NN layers, the required number of epochs increases due to the smaller local accuracy $\gamma_L \simeq 0.1$ as well as the larger number of parameters to be trained for each NN layer. Finally, for the proposed setup, we noticed that performance improves by keeping the learning rate $\mu_t\beta_{k,i}$ for the hidden layer parameters $[\mathbf{w}_{0,1}^T, \mathbf{w}_{1,1}]$, ($q = 1$) slightly larger than the rate for the output layer parameters $[\mathbf{w}_{0,2}^T, \mathbf{w}_{1,2}]$, ($q = 2$). This is particularly evident when convolutional layers are used.

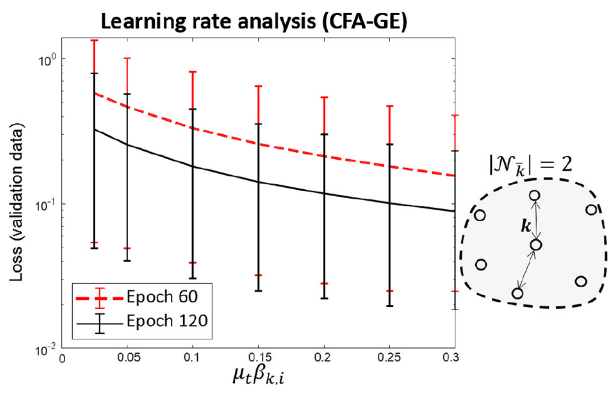

(a)

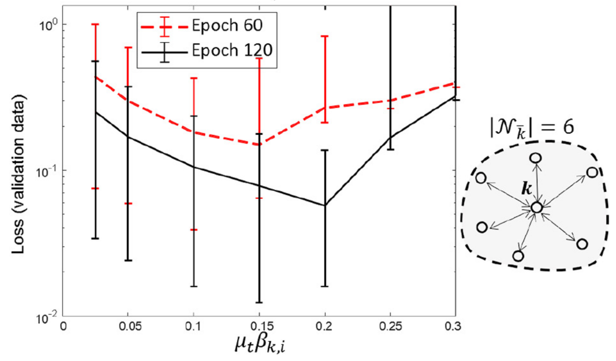

(b)

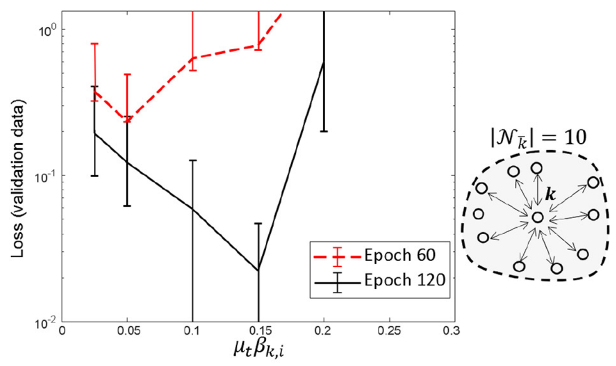

(c)

Fig. 7. Validation loss for varying rates ($\mu_t\beta_{k,i}$) for $K = 80$ devices and k-regular networks with varying connectivity, ranging from a) $|\mathcal{N}_{\bar{k}}| = 2$, b) $|\mathcal{N}_{\bar{k}}| = 6$ up to c) $|\mathcal{N}_{\bar{k}}| = 10$.

C. Communication and Computational Cost Assessment

The CFA-GE method achieves the performance of the centralized ML without federation, in exchange for a more intensive use of D2D wireless links and local computations, that scale in both cases with the number of neighbors $|\mathcal{N}_{\bar{k}}|$. Based on the analysis in Section III-D, in Table IV we compare the communication overhead and computational cost for varying number of neighbors $|\mathcal{N}_k|$, considering FA, CFA, and CFA-GE methods. In particular, the communication overhead quantifies the number of bytes that need to be transmitted over the air by each device every communication/consensus round. The computational cost is measured in terms of average local execution time per communication round and device.

The communication overhead of FA and CFA is 2.98 kB/round/device for CNN and 33.36 kB/round/device for 2NN.

TABLE IV
COMMUNICATION OVERHEAD [KB/ROUND/DEVICE] AND COMPUTATIONAL COST—AVERAGE EXECUTION TIME [M.SEC./ROUND/DEVICE] MEASURED ON THE DEVICE

		Comm. overhead [Kbyte/round/device]		Execution time (avg.) [m.sec./round/device]	
$|\mathcal{N}_{\bar{k}}|$		CNN	2NN	CNN	2NN
2	FA	2.98	33.36	140ms	145ms
	CFA	2.98	33.36	141ms	146ms
	CFA-GE	5.96	66.72	321ms	334ms
6	FA	2.98	33.36	140ms	145ms
	CFA	2.98	33.36	142ms	147ms
	CFA-GE	17.88	200.16	684ms	711ms
10	FA	2.98	33.36	140ms	145ms
	CFA	2.98	33.36	149ms	153ms
	CFA-GE	29.8	333.7	984ms.	∼ 1sec.

Overhead corresponds in both cases to the model **W** size: this is evaluated according to the model parameters highlighted in Table I and assuming 16 bit/parameter quantization. CFA-GE overhead is larger as it scales linearly with $|\mathcal{N}_k|$, therefore, it can be quantified as $2.98 \cdot |\mathcal{N}_k|$ kB/round/device for CNN and $33.36 \cdot |\mathcal{N}_k|$ kB/round/device for 2NN. Notice that bandwidth-limited communication systems, e.g., based on IEEE 802.15.4, 6LoWPAN, and related evolutions [14]–[34], are characterized by small physical frame payloads, typically below 1 kB/frame. Therefore, sending FA, CFA, or CFA-GE parameters on each round might require the aggregation of consecutive physical frames, or multiple network layer transactions. For comparison with centralized ML, FFT training measurements collected individually by devices have size within the range $1 \div 4$ MB, assuming 32 bit quantization for in-phase (I) and quadrature (Q) components.

Local execution time considers here the ML stages only, while data preprocessing and acquisition steps are not included, being negligible compared to the learning steps. The execution time shown in Table IV is measured using the *timeit* Python module, on a device equipped with a 1.5-GHz quad-core ARM Cortex-A72 processor with 4-GB internal RAM.[6] Focusing on a realistic IIoT environment, the device has thus limited computational capabilities, compared with the server. Execution time depends in general on the specific CPU or tensor processing unit (TPU) performances; nevertheless, the analysis of the results in Table IV is useful to highlight the scaling performance of the proposed methods compared to the plain FA algorithm. Considering FA, the execution time on the device is ruled by local SGD rounds: it is 140 and 145 ms for CNN and 2NN, respectively. Notice that FA needs the server for aggregation, while such additional cost is not considered here. Compared with FA, CFA adds a model aggregation stage (8) for each NN layer that takes 0.5 ms on average per neighbor. Finally, CFA-GE adds a cumulative time of 90 ms for CNN and 94 ms for 2NN on average per neighbor. This is needed for the computation of one additional gradient, the MEWMA update (17), and one SGD round (19) per neighbor.

[6]Typical commercial low-power single-board computer (Raspberry Pi 4 Model B): smaller execution times are expected when running on dedicated TPU processors.

Considering both overhead and local execution time, CFA-GE cost per round is higher compared with CFA and FA and scales almost linearly with the number of neighbors $|\mathcal{N}_{\bar{k}}|$. CFA total cost is instead comparable with FA when $|\mathcal{N}_{\bar{k}}| < 10$. However, it is worth to notice that, as shown by the numerical results in Section V-B, CFA-GE only needs $|\mathcal{N}_{\bar{k}}| = 2$ neighbors for convergence and even with such a low degree of cooperation, it reduces the number of rounds by almost one order of magnitude (Fig. 6) compared to CFA. Using more than $|\mathcal{N}_{\bar{k}}| = 2$ cooperating neighbors for CFA-GE provides only marginal improvements and it is thus not recommended. Having said that, we can conclude that CFA-GE is promising as an effective replacement for FA and centralized ML when it is critical to limit the number of communication rounds, or in case frequent learning updates are needed. CFA keeps complexity and overhead comparable with FA in exchange for more rounds. It is thus suitable for noncritical learning tasks and it can support bandwidth-limited D2D communication systems characterized by small frame payloads.

VI. Conclusion

This article addressed a new family of FL methods that leverage the mutual cooperation of devices in distributed wireless IoT networks without relying on the support of a central coordinator. The adaptation of FA, namely, the CFA method, was first discussed to exploit distributed consensus paradigms for FL. Next, to improve convergence speed, we proposed a new algorithm based on iterative exchange of model updates and gradients. The CFA-GE algorithm was optimized for two-stage gradient negotiations so that it can be tailored to arbitrarily large-scale networks.

The proposed distributed learning approach was validated on an IIoT scenario where an NN model was distributedly trained to solve the problem of passive body detection inside a human–robot collaborative workspace. CFA-GE was shown to achieve the performance of server-side (or centralized) federated optimization. Decentralized optimization is fully serverless with respect to the NN model training as intelligence is pushed down into the IoT devices. This is particularly effective when direct communication with the infrastructure is reserved for critical tasks (e.g., to control the robot or to perform safety tasks). Motivated by the growing range of ML applications that will be deployed in 5G and beyond wireless networks, FL via consensus emerges in this article as a promising framework for flexible model optimization over networks characterized by decentralized connectivity patterns as in massive IoT implementations.

Despite the promising features, the proposed consensus-based approach gives rise to new challenges, which need to be taken into account during the system deployment. For example, this article considered a simple enough NN model for optimization running on IoT devices with limited computation capabilities. However, training of deeper networks on constrained devices is expected to become the mainstream in the near future [48]. Application of consensus-based federated optimization to deeper networks might require a more efficient use of the limited bandwidth, including quantization, compression, or *ad hoc* channel encoding [47]. As revealed in the considered case study, tweaking of the model hyperparameters [16] as well as optimizing the learning rates for each NN model layer separately are also viable solutions to limit the number of communication rounds. Finally, although this article addressed a classification task as application of federated optimization, both CFA and CFA-GE can be generalized to perform a wider range of computations.

Appendix A
Comparing CFA and CFA-GE

Combining (13) and (14), we obtain the update equation for CFA-GE

$$\mathbf{W}_{t+1,k} = \underbrace{\boldsymbol{\psi}_{t,k} - \mu_t \sum_{i\in\mathcal{N}_{\bar{k}}} \beta_{t,i}\nabla L_{t,i}(\boldsymbol{\psi}_{t,k})}_{\widetilde{\boldsymbol{\psi}}_{t,k}} - \mu_t\beta_{t,k}\big[\nabla L_{t,k}(\widetilde{\boldsymbol{\psi}}_{t,k})\big] \tag{22}$$

with $\boldsymbol{\psi}_{t,k}$ in (8). This is comparable with the CFA approach in (9). Unlike CFA, gradient exchange terms $\sum_{i\in\mathcal{N}_{\bar{k}}} \beta_{t,i}\nabla L_{t,i}(\boldsymbol{\psi}_{t,k})$ allow to incorporate the influence of training data collected by the neighborhood of device k through the gradient terms $L_{t,i}(\boldsymbol{\psi}_{t,k})$. Computation of $\widetilde{\boldsymbol{\psi}}_{t,k}$ (13) thus corresponds to an initial gradient descent round using the training data from the neighborhood, while subsequent rounds (22) are performed using SGD over local data minibatches.

Appendix B
Application to SGD With momentum

SGD is considered throughout this article as a popular optimization strategy; however, it shows slow convergence properties in some ML problems [10]. Recently, the method of momentum inspired several algorithms (such as RMSProp and Adam [41]) optimized for accelerated learning. Considering that in federated optimization any improvement in the convergence speed is beneficial in terms of bandwidth usage and latency, we address the necessary adaptations of the CFA-GE strategy to leverage momentum information. With respect to SGD, momentum addresses the problem of imperfect estimation of the stochastic gradients as well as the conditioning of the Hessian matrix [32]. Poor estimation of gradients is even more critical when considering distributed learning setups. Compared with SGD, the use of momentum modifies the local update rule (9), (14) as

$$\begin{cases} \mathbf{W}_{t+1,k} = \boldsymbol{\psi}_{t,k} + \nu_{t+1,k} \\ \nu_{t+1,k} = \varrho\nu_{t,k} - \mu_t\nabla L_{t,k}(\boldsymbol{\psi}_{t,k}) \end{cases} \tag{23}$$

where both current and past gradients contribute to the local model update (for device k) as multiplied by an exponentially decaying function ruled by hyperparameter $\varrho \in [0, 1)$. $\nu_{t,k}$ is the momentum, or velocity, of the gradient descent particle at round t, that is stored by device k.

Momentum-based techniques can be used seamlessly combined with CFA by simply replacing (9) with (23) as gradient sharing is not permitted. Considering that in CFA-GE local gradients are exchanged among neighbors, some necessary adaptations are required to leverage momentum. The received gradients, i.e., at epoch $t-1$, are now used for local momentum update as

$$\nu_{t,k} = \varrho \nu_{t-1,k} - \mu_t \sum_{i \in \mathcal{N}_{\bar{k}}} \beta_{k,i} \mathcal{P}_\Theta \left[\overline{\nabla L}_{t-1,i} \right]. \tag{24}$$

We then replace (19) with $\widetilde{\boldsymbol{\psi}}_{t,k} = \boldsymbol{\psi}_{t,k} + \nu_{t,k}$ and (14) with (23). The use of the Nesterov momentum [32] policy requires minor adaptations: the devices should now exchange the parameters $\Theta_{t,k} := [\boldsymbol{\psi}_{t,k} + \varrho \nu_{t-1,k}, \nabla \mathbf{L}_{t,k}]$. These are: the local model $\boldsymbol{\psi}_{t,k} + \varrho \nu_{t-1,k}$ *after* applying the velocity term (24) and the gradients $\nabla \mathbf{L}_{t,k} := \{ \overline{\nabla L}_{t,k}(\boldsymbol{\psi}_{t-1,i}) \; \forall i \in \mathcal{N}_{\bar{k}} \}$ described as

$$\begin{aligned} \overline{\nabla L}_{t,k}(\boldsymbol{\psi}_{t-1,i}) &= \varrho \nabla L_{t,k}(\boldsymbol{\psi}_{t-1,i} + \varrho \nu_{t-1,i}) \\ &\quad + (1-\varrho) \overline{\nabla L}_{t-1,k} \end{aligned} \tag{25}$$

that replace the terms in (17).

REFERENCES

[1] C. Zhang, P. Patras, and H. Haddadi, "Deep learning in mobile and wireless networking: A survey," *IEEE Commun. Surveys Tuts.*, vol. 21, no. 3, pp. 2224–2287, 3rd Quart., 2019.

[2] W. G. Hatcher and W. Yu, "A survey of deep learning: Platforms, applications and emerging research trends," *IEEE Access*, vol. 6, pp. 24411–24432, 2018.

[3] S. Savazzi, S. Sigg, F. Vicentini, S. Kianoush, and R. Findling, "On the use of stray wireless signals for sensing: A look beyond 5G for the next generation of industry," *Computer*, vol. 52, no. 7, pp. 25–36, Jul. 2019.

[4] K. M. Alam and A. El Saddik, "C2PS: A digital twin architecture reference model for the cloud-based cyber-physical systems," *IEEE Access*, vol. 5, pp. 2050–2062, 2017.

[5] S. Samarakoon, M. Bennis, W. Saad, and M. Debbah, "Federated learning for ultra-reliable low-latency V2V communication," in *Proc. IEEE Globecom*, 2018, pp. 1–7.

[6] M. Bennis, M. Debbah, and H. V. Poor, "Ultrareliable and low-latency wireless communication: Tail, risk, and scale," *Proc. IEEE*, vol. 106, no. 10, pp. 1834–1853, Oct. 2018.

[7] J. Konečn *et al.*, "Federated optimization: Distributed machine learning for on-device intelligence," *CoRR*, 2016. [Online]. Available: http://arxiv.org/abs/1610.02527

[8] S. Wang *et al.*, "Adaptive federated learning in resource constrained edge computing systems," *IEEE J. Sel. Areas Commun.*, vol. 37, no. 6, pp. 1205–1221, Jun. 2019.

[9] J. Konečný *et al.*, "Federated learning: Strategies for improving communication efficiency," *CoRR*, 2016. [Online]. Available: http://arxiv.org/abs/1610.05492

[10] L. Bottou, "Large-scale machine learning with stochastic gradient descent," in *Proc. COMPSTAT*, 2010, pp. 1529–1541.

[11] G. Aloi, O. Briante, M. Di Felice, G. Ruggeri, and S. Savazzi, "The SENSE-ME platform: Infrastructure-less smartphone connectivity and decentralized sensing for emergency management," *Pervasive Mobile Comput.*, vol. 42, pp. 187–208, Dec. 2017.

[12] S. Kianoush, M. Raja, S. Savazzi, and S. Sigg, "A cloud-IoT platform for passive radio sensing: Challenges and application case studies," *IEEE Internet Things J.*, vol. 5, no. 5, pp. 3624–3636, Oct. 2018.

[13] M. Brambilla, M. Nicoli, G. Soatti, and F. Deflorio, "Augmenting vehicle localization by cooperative sensing of the driving environment: Insight on data association in urban traffic scenarios," *IEEE Trans. Intell. Transp. Syst.*, to be published.

[14] L. Ascorti, S. Savazzi, G. Soatti, M. Nicoli, E. Sisinni, and S. Galimberti, "A wireless cloud network platform for industrial process automation: Critical data publishing and distributed sensing," *IEEE Trans. Instrum. Meas.*, vol. 66, no. 4, pp. 592–603, Apr. 2017.

[15] B. McMahan, E. Moore, D. Ramage, S. Hampson, and B. A. Y. Arcas, "Communication-efficient learning of deep networks from decentralized data," in *Proc. 20th Int. Conf. Artif. Intell. Stat.*, vol. 54, 2017, pp. 1273–1282.

[16] E. Jeong, S. Oh, H. Kim, J. Park, M. Bennis, and S.-L. Kim, "Communication-efficient on-device machine learning: Federated distillation and augmentation under non-IID private data," in *Proc. NIPS Workshop*, Montreal, QC, Canada, 2018. [Online]. Available: https://arxiv.org/abs/1811.11479

[17] M. Blot, D. Picard, M. Cord, and N. Thome, "Gossip training for deep learning," in *Proc. 30th Conf. Neural Inf. Process. Syst. (NIPS)*, Barcelona, Spain, 2016. [Online]. Available: https://arxiv.org/abs/1611.09726

[18] J. A. Daily *et al. GossipGrad: Scalable Deep Learning Using Gossip Communication Based Asynchronous Gradient Descent*. Accessed: Dec. 15, 2019. [Online]. Available: https://arxiv.org/abs/1803.05880

[19] A. Guha, S. Siddiqui, S. Polsterl, N. Navab, and C. Wachinger. *BrainTorrent: A Peer-to-Peer Environment for Decentralized Federated Learning*. Accessed: Dec. 15, 2019. [Online]. Available: https://arxiv.org/abs/1905.06731

[20] C. Hu, J. Jiang, and Z. Wang, "Decentralized federated learning: A segmented gossip approach," in *Proc. 1st Int. Workshop Fed. Mach. Learn. User Privacy Data Confidentiality (FML)*, 2019. [Online]. Available: https://arxiv.org/abs/1908.07782

[21] A. Lalitha, S. Shekhar, T. Javidi, and F. Koushanfar, "Fully decentralized federated learning," in *Proc. 3rd Workshop Bayesian Deep NIPS Workshop*, 2018, pp. 1–9.

[22] A. Lalitha, O. C. Kilinc, T. Javidi, and F. Koushanfar. *Peer-to-Peer Federated Learning on Graphs*. [Online]. Available: https://arxiv.org/abs/1901.11173

[23] G. Soatti, M. Nicoli, S. Savazzi, and U. Spagnolini, "Consensus-based algorithms for distributed network-state estimation and localization," *IEEE Trans. Signal Inf. Process. Netw.*, vol. 3, no. 2, pp. 430–444, Jun. 2017.

[24] C. Ma *et al.*, "Distributed optimization with arbitrary local solvers," *Optim. Methods Softw.*, vol. 32, no. 4, pp. 813–843, 2017.

[25] Y. Zhang and X. Lin, "DiSCO: Distributed optimization for self-concordant empirical loss," in *Proc. ICML*, 2015, pp. 362–370.

[26] M. G. Rabbat and R. D. Nowak, "Quantized incremental algorithms for distributed optimization," *IEEE J. Sel. Areas Commun.*, vol. 23, no. 4, pp. 798–808, Apr. 2005.

[27] I. D. Schizas, A. Ribeiro, and G. B. Giannakis, "Consensus in ad hoc WSNs with noisy links—Part I: Distributed estimation of deterministic signals," *IEEE Trans. Signal Process.*, vol. 56, no. 1, pp. 350–364, Jan. 2008.

[28] R. Olfati-Saber, A. Fax, and R. M. Murray, "Consensus and cooperation in networked multi-agent systems," *Proc. IEEE*, vol. 98, no. 7, pp. 1354–1355, Jan. 2010.

[29] F. S. Cattivelli and A. H. Sayed, "Analysis of spatial and incremental LMS processing for distributed estimation," *IEEE Trans. Signal Process.*, vol. 59, no. 4, pp. 1465–1480, Apr. 2011.

[30] J. Chen and A. H. Sayed, "Diffusion adaptation strategies for distributed optimization and learning over networks," *IEEE Trans. Signal Process.*, vol. 60, no. 8, pp. 4289–4305, Aug. 2012.

[31] A. H. Sayed, S.-Y. Tu, J. Chen, X. Zhao, and Z. J. Towfic, "Diffusion strategies for adaptation and learning over networks: An examination of distributed strategies and network behavior," *IEEE Signal Process. Mag.*, vol. 30, no. 3, pp. 155–171, May 2013.

[32] I. Sutskever, J. Martens, G. Dahl, and G. Hinton, "On the importance of initialization and momentum in deep learning," in *Proc. 30th Int. Conf. Mach. Learn.*, Atlanta, GA, USA, 2013, pp. 1139–1147.

[33] M. Abadi *et al.* (2015). *TensorFlow: Large-Scale Machine Learning on Heterogeneous Systems*. [Online]. Available: http://tensorflow.org/

[34] M. R. Palattella *et al.*, "Internet of Things in the 5G era: Enablers, architecture, and business models," *IEEE J. Sel. Areas Commun.*, vol. 34, no. 3, pp. 510–527, Mar. 2016.

[35] S. Savazzi, V. Rampa, and U. Spagnolini, "Wireless cloud networks for the factory of things: Connectivity modeling and layout design," *IEEE Internet Things J.*, vol. 1, no. 2, pp. 180–195, Apr. 2014.

[36] S. Kianoush, S. Savazzi, and V. Rampa, "Passive detection and discrimination of body movements in the sub-THz band: A case study," in *Proc. IEEE Int. Conf. Acoust. Speech Signal Process. (ICASSP)*, Brighton, U.K., May 2019, pp. 1597–1601.

[37] E. Soltanmohammadi, K. Ghavami, and M. Naraghi-Pour, "A survey of traffic issues in machine-to-machine communications over LTE," *IEEE Internet Things J.*, vol. 3, no. 6, pp. 865–884, Dec. 2016.

[38] A. Øland and B. Raj, "Reducing communication overhead in distributed learning by an order of magnitude (almost)," in *Proc. IEEE Int. Conf. Acoust. Speech Signal Process. (ICASSP)*, Brisbane, QLD, Australia, 2015, pp. 2219–2223.

[39] M. N. Tehrani, M. Uysal, and H. Yanikomeroglu, "Device-to-device communication in 5G cellular networks: Challenges, solutions, and future directions," *IEEE Commun. Mag.*, vol. 52, no. 5, pp. 86–92, May 2014.

[40] Y. LeCun, L. Bottou, Y. Bengio, and P. Haffner, "Gradient-based learning applied to document recognition," *Proc. IEEE*, vol. 86, no. 11, pp. 2278–2324, Nov. 1998.

[41] D. P. Kingma and J. Ba, "Adam: A method for stochastic optimization," in *Proc. 3rd Int. Conf. Learn. Represent. (ICLR)*, San Diego, CA, USA, 2015. [Online]. Available: https://arxiv.org/abs/1412.6980

[42] S. Savazzi, V. Rampa, F. Vicentini, and M. Giussani, "Device-free human sensing and localization in collaborative human–robot workspaces: A case study," *IEEE Sensors J.*, vol. 16, no. 5, pp. 1253–1264, Mar. 2016.

[43] Z. Zhang, Z. Tian, and M. Zhou, "Latern: Dynamic continuous hand gesture recognition using FMCW radar sensor," *IEEE Sensors J.*, vol. 18, no. 8, pp. 3278–3289, Apr. 2018.

[44] B. Vandersmissen *et al.*, "Indoor person identification using a low-power FMCW radar," *IEEE Trans. Geosci. Remote Sens.*, vol. 56, no. 7, pp. 3941–3952, Jul. 2018.

[45] SiliconRadar. (Nov. 2018). *120-GHz Highly Integrated IQ Transceiver With Antennas on Chip in Silicon Germanium Technology*. Accessed: Aug. 26, 2019. [Online]. Available: https://siliconradar.com/datasheets/Datasheet_TRA_120_002_V0.8.pdf

[46] Data Repository. (2019). *Federated Learning: Example Dataset (FMCW 122GHz Radars)*. Accessed: Sep. 23, 2019. [Online]. Available: https://github.com/labRadioVision/federated

[47] M. M. Amiri and D. Gündüz, "Machine learning at the wireless edge: Distributed stochastic gradient descent over-the-air," *CoRR*, vol. abs/1901.00844, 2019. [Online]. Available: http://arxiv.org/abs/1901.00844

[48] N. D. Lane, S. Bhattacharya, A. Mathur, P. Georgiev, C. Forlivesi, and F. Kawsar, "Squeezing deep learning into mobile and embedded devices," *IEEE Pervasive Comput.*, vol. 16, no. 3, pp. 82–88, Jul. 2017.

Stefano Savazzi (Member, IEEE) received the M.Sc. degree (Hons.) in telecommunication engineering and the Ph.D. degree (Hons.) in information technology from the Politecnico di Milano, Milan, Italy, in 2004 and 2008, respectively.

In 2012, he joined the Institute of Electronics, Computer and Telecommunication Engineering, Consiglio Nazionale delle Ricerche, Milan, as a Researcher. He has coauthored over 100 scientific publications, including journals, conferences, and book chapters. He was a Visiting Researcher with Uppsala University, Uppsala, Sweden, in 2005; the University of California San Diego, La Jolla, CA, USA, in 2007; and ftw, Vienna, Austria, in 2010. His current research interests include signal processing, machine learning and networking design aspects for the Internet of Things, cooperative and cognitive sensor networks for radio vision and localization.

Dr. Savazzi won the Dimitris N. Chorafas Foundation Award for best Ph.D. dissertation. He is serving as a Topic Editor for *Sensors Journal* (MDPI).

Monica Nicoli (Member, IEEE) received the M.Sc. degree (Hons.) in telecommunication engineering and the Ph.D. degree in electronic and communication engineering from Politecnico di Milano, Milan, Italy, in 1998 and 2002, respectively.

She was a Visiting Researcher with Uppsala University, Uppsala, Sweden, in 2001. In 2002, she joined the Politecnico di Milano, as a faculty member, where she is currently an Associate Professor. She has coauthored over 100 scientific publications. Her research interests are in the area of statistical signal processing and wireless communications, with a focus on localization, smart mobility, cooperative and distributed systems for the Internet of Things/Vehicles.

Dr. Nicoli is a recipient of the 1999 Marisa Bellisario Award, and the 1999 SPE-EAGE Best Thesis Award, and a co-recipient of the Best Paper Awards of the IEEE Statistical Signal Processing Workshop 2018 and the IET ITS Journal 2014. She served as an Associate Editor for the *EURASIP Journal on Wireless Communications and Networking* from 2010 to 2017, and a Lead Guest Editor for the Special Issue on Localization in Mobile Wireless and Sensor Networks in 2011.

Vittorio Rampa (Member, IEEE) received the degree (Hons.) in electronics engineering from the Politecnico di Milano, Milan, Italy, in 1984.

In 1986, he joined the Consiglio Nazionale delle Ricerche of Italy, Milan, as a Researcher. From 1999 to 2014, he was an Adjunct Professor with the Politecnico di Milano, where he taught courses on software-defined radios and radio localization systems. In 2001, he became a Senior Researcher with the Institute of Electronics, Computer and Telecommunication Engineering. He has coauthored more than 80 scientific publications, including journals, conferences, patents, books and book chapters. His main research interests include signal processing algorithms and architectures for wireless communications, machine and deep learning algorithms for sensor networks, radio vision models, algorithms and systems, and virtual instrumentation techniques for test and verification of wireless systems.